Electronic Supplementary Information

Oxygen spillover engineering design in atomically dispersed sites for high-efficiency photoproduction of hydrogen peroxide from water

Xueming Dang,†[a] Shuai Wu,†[b] Qian Li,†[c] Xiaorong Gan,[d] Alex K.-Y. Jen,[c,e] Dangyuan Lei,*[c,f] Huimin Zhao*[a]

[a] Key Laboratory of Industrial Ecology and Environmental Engineering (Ministry of Education China), School of Environmental Science and Technology, Dalian University of Technology, Dalian, 116024, China.

[b] Center for Water and Ecology, State Key Joint Laboratory of Environment Simulation and Pollution Control, School of Environment, Tsinghua University, Beijing, 100084, China.

[c] Department of Materials Science and Engineering, City University of Hong Kong, Hong Kong, 999077, China.

[d] Key Laboratory of Integrated Regulation and Resource Development on Shallow Lake of Ministry of Education, College of Environment, Hohai University, Nanjing, 210098, China.

[e] Department of Chemistry, City University of Hong Kong, Hong Kong, 999077, China.

[f] Department of Physics, Centre for Functional Photonics, Hong Kong Branch of National Precious Metals Material Engineering Research Centre, and Hong Kong Institute of Clean Energy, City University of Hong Kong, Hong Kong, 999077, China.

† X. D., S. W. and Q. L. contributed equally to this work.

* Corresponding authors Email: zhaohuim@dlut.edu.cn; dangylei@cityu.edu.hk

Table of Contents for Electronic Supplementary Information

1. Experimental Section

1.1 Chemicals and materials

The following reagents were used in fabrication of photocatalysts, measurement of H_2O_2 concentration and investigation of H_2O_2 generation procedure: 1,4-dioxane, 1,3,5-triformylphloroglucinol, 3,9-diamino-benzo[1,2-b:4,5-b'] bis[1]benzothiophene-5,5,11,11-tetraoxide, horseradish peroxidase (HRP), N, N-dimethylformamide (DMF), cefalexin, 5,5-dimethyl-1-pyrroline N-oxide (DMPO), orange II, $KBrO_3$, p-benzoquinone (p-BQ), p-tert-butanol (TBA), nitro blue tetrazolium (NBT), 2,2,6,6-tetramethylpiperidine (TEMP) and water-^{18}O ($H_2{}^{18}O$) (Shanghai Aladdin Bio-Chem Technology Co., Ltd., China); Monometallic sodium orthophosphate (NaH_2PO_4), dibasic sodium phosphate (Na_2HPO_4), sodium sulfate (Na_2SO_4), hydrogen peroxide (H_2O_2) solution (30%, wt.%), acetone and ethanol absolute, citric acid, melamine, dichloromethane, isopropanol, methanol (MeOH), ethylenediaminetetraacetic acid disodium salt (EDTA-2Na), nickel chloride hexahydrate ($NiCl_3 \cdot 6H_2O$) and sodium periodate ($NaIO_4$) (Tianjin Bodi chemical Co., Ltd., China); N, N-diethyl p-phenylenediamine sulfate (DPD) (Tianjin Guangfu Fine Chemical Research Institute, China); Manganese dioxide (MnO_2) and ferrous sulfate ($FeSO_4$) (Tianjin Damao Chemical Reagent Factory, China); Magnesium nitrate ($Mg(NO_3)_2$) (Tianjin Dingshengxin Chemical Industry Co., Ltd., China) Phosphate buffer saline (PBS) (Beijing Solarbio Science & Technology Co., Ltd., China); Ultrapure water was received from purification system (Millipore; ≥18 MΩ). Tap water, lake water and sea water were obtained from local laboratory, Xishan lake (Dalian, China) and yellow sea.

1.2. Characterization instruments

X-ray powder diffraction (XRD) pattern was recorded by a D8 Advance X-

ray diffractometer with Cu Kα radiation, λ = 1.5406 Å (Bruker, Germany). Scanning electron microscopy (SEM) images were recorded on an S-4800 field emission scanning electron microscope (Hitachi, Japan). Transmission electron microscopy (TEM) equipped with energy dispersive X-ray spectroscopy (EDS, X-MAX20) were recorded on a JEM F200 transmission electron microscope (JEOL, Japan). Ultraviolet-visible diffuse reflectance spectra (UV-Vis DRS) were performed by a V-550 spectrometer (Shimadzu, Japan). Photoluminescence (PL) spectra were measured on a Hitachi F-7600 spectrophotometer (Japan). X-ray photoelectron spectroscopy (XPS) was recorded by a Thermos Scientific K-Alpha+ instrument with Al Kα X-ray irradiation (UK). The aberration-corrected high-angle annular dark field transmission electron microscopy (HAADF-TEM) was conducted on a FEI Titan G2 60-300 microscope (USA) with a Schottky cold-field emission gun. The Ni K-edge X-ray absorption study was performed at the BL14B2 of SPring-8 station (Japan). The inductively coupled plasma (ICP) spectroscopy analysis was conducted on a Optima2000DV instrument (USA). The femtosecond transient absorption (fs-TA) spectra were measured with a commercial TA system (TA100, Time-Tech Spectra, China). Electron paramagnetic resonance (EPR) spectra were recorded on a E500 EPR spectrometer (Bruker, Germany). In-situ Raman spectra were collected on an inVia Qontor confocal micro Raman spectrometer (Renishaw PLC, England). Gas chromatography-mass spectrometry (GC-MS) analysis was conducted using the Shimadzu GCMS-QP2020 instrument (Japan).

1.3. Synthesis of COFs

Firstly, 10.5 mg 1,3,5-triformylphloroglucinol and 28.8 mg 3, 9-diamino-benzo[1,2-b:4,5- b']bis[1]benzothiophene-5,5,11,11-tetraoxide were added in a mixture

solution with 1.5 mL 1,4-dioxane, 1.5 mL mesitylene and 0.3 mL acetic acid (3 mol L^{-1}). After the sonication for 10 min, the mixture was degassed with a vacuum pump. Then the sample was put into a refrigerator at -80 ℃ for freezing. The degassed procedure was further performed in the thawing of mixture. After three freeze-thaw cycles, mixture was kept at 120 ℃ under a vacuum environment for three days. The obtained solid was washed with N, N-dimethylformamide and acetone for several times. Finally, the red sample was dried by a vacuum freezing process.

1.4. Synthesis of Ni-CDs

The Ni single atom anchored carbon dots (Ni-CDs) were fabricated via a microwave heat-treatment method. 3 g citric acid, 1 g urea and 0.5 g $NiCl_2 \cdot 6H_2O$ were dissolved in 8 mL ultrapure water under vigorously stirring. Then, the transparent solution was moved into the microwave digestion tank and reacted for 10 min with power mode of 600 W. After the reaction, the colorless liquid was transformed into a dark brown solid. Subsequently, the solid was heated at 80 ℃ for 12 h to remove small residual molecules. The mixture was then dispersed in ultrapure water and centrifuged at 9000 rpm for 1 h to remove agglomerated large particles. The obtained brown solution was further eluted via a mixture of dichloromethane and methanol with a volume ratio of 1:1. The dialysis of solution was further performed with the dialysis tube (1000 molecular weight for trapped molecule) in ultrapure water. The resultant product was obtained after the vacuum freezing drying. The CDs were prepared through above procedure without the addition of Ni-containing precursor.

1.5. Synthesis of Ni-CDs/COFs

The 28 mg COFs were dispersed in 10 mL DMF under ultrasonic irradiation. Then 2 mg Ni-CDs were added into the above solution under vigorously stirring for 1 h. The resulting mixture was dried at 80 ℃ to completely evaporate DMF. The solid was

174 further washed with ultrapure water and centrifuged at 9000 rpm for 10 min. The final
175 powder was obtained after drying at 80 ℃ and denoted as Ni-CDs/COFs. The hybrid
176 of COFs and CDs was further prepared and named as CDs/COFs.

177 **1.6. Photocatalytic H_2O_2 production reaction**

178 The 10 mg photocatalyst was added in 50 mL of ultrapure water and ultrasonically
179 dispersed for 20 min. Then the suspension was continuously filled with O_2 and kept
180 stirring for another 20 min in dark. After that, the reaction solution was irradiated under
181 a Xenon lamp (PLS-SXE300D/DUV, Perfect light) with a 420 nm cutoff film. The
182 reaction temperature of mixture was controlled at 25 ℃ under a circulating water.
183 During the catalytic process, 2.5 mL of reaction solution was taken out every 10 min
184 and filtrated through a 0.22 μm PES filter to remove photocatalyst. The concentration
185 of H_2O_2 was measured by an enzyme-based colorimetric method. Sodium phosphate
186 buffer was prepared through mixing 87.7 mL NaH_2PO_4 solution (1 mol L^{-1}), 12.6 mL
187 Na_2HPO_4 solution (1 mol L^{-1}) in 99.7 mL ultrapure water. The N, N-diethyl p-
188 phenylenediamine sulfate (DPD) solution and horseradish peroxidase (HRP) solution
189 were prepared by adding 0.1 g DPD in 10 mL sulfuric acid (H_2SO_4) solution (0.1 mol
190 L^{-1}) and 3 mg HRP in 3 mL ultrapure water. For the H_2O_2 concentration test process,
191 0.4 mL sodium phosphate buffer, 0.05 mL DPD solution and 0.05 mL HRP solution
192 were mixed with 2 mL filtered sample and kept 90 s. The content of generated H_2O_2
193 was then determined at 551 nm over a SP-756P UV-vis spectrophotometer.

194 **1.7. Measurement of apparent quantum yield**

195 The apparent quantum yield (AQY) of Ni-CDs/COFs was measured under Xenon
196 lamp irradiation with single-wavelength light at 420 nm, 500 nm, 550 nm, 600 nm, 650
197 nm and 700 nm. The photocatalytic reaction was performed at 25 ℃ in ultrapure water.
198 The AQY was calculated based on the following Equation (S1).[1,2]

$$AQY = \frac{(number\ of\ H_2O_2\ production) \times 2}{number\ of\ incident\ photons} \times 100\%$$

$$= \frac{2 \times N_a \times M}{\frac{P \times S \times t \times \lambda}{h \times c}} = \frac{2 \times N_a \times M \times h \times c}{S \times P \times t \times \lambda}$$

Where N_a is the Avogadro constant (6.022×10^{23} mol^{-1}), M is the amount of produced H_2O_2 molecule (mol), h is the Plank's constant (6.626×10^{-34} J s), c is the speed of light in free space (3×10^8 m s^{-1}), S is the irradiation area (1×10^{-4} m^2), P is the intensity of irradiation light (16.2 mW cm^{-2} at 429 nm), t is the photoreaction time (s), λ is the wavelength length of the monochromatic light (m).

1.8. Determination of solar-to-chemical conversion efficiency

The solar-to-chemical conversion (SCC) efficiency was evaluated using a Xe lamp with an AM 1.5G filter as simulated natural light source and calculated according to the following Equation (S2)[3,4]:

$$SCC\ (\%) = \frac{(\triangle G\ for\ H_2O_2\ generation) \times (number\ of\ formed\ H_2O_2)}{P \times t} \times 100\%$$

$$= \frac{\triangle G \times M}{P \times t} \times 100\%$$

Where ΔG = 117 kJ mol^{-1}, M is the amount of formed H_2O_2 molecule (mol), P is the total input power (W), t is the reaction time (s).

1.9. Photocatalytic decomposition of H_2O_2

The photocatalytic decomposition of H_2O_2 was measured with addition of 10 mg photocatalyst in 50 mL H_2O_2 aqueous solution (10 mmol L^{-1}). The light source and reaction temperature in H_2O_2 decomposition measurement was the same as those in H_2O_2 production test. During the decomposition reaction, 2.5 mL sample collected every 10 min and was filtered to remove photocatalyst. The H_2O_2 concentration was measured using the enzyme-based colorimetric method.

1.10. Mott-Schottky measurement

Mott-Schottky curves were tested with a frequency of 1000 Hz, 1500 Hz and 2000 Hz in a 0.1 mol L^{-1} Na_2SO_4 solution. Then the potentials of flat band of photocatalysts were obtained by fitting the curves and transformed to the value (vs normal hydrogen electrode (NHE)) based on the equation (S3) and equation (S4).[5-7]

$$(RHE) = E(SCE) + 0.0591\ pH + 0.24 \qquad \text{Equation (S3)}$$

$$E(RHE) = E(NHE) + 0.0591\ pH \qquad \text{Equation (S4)}$$

1.11. Photoelectrochemical measurement

The electrochemical impedance spectroscopy (EIS) was measured on a PARSTAT 2273 electrochemical system (Princeton, USA) with frequency of 0.1 Hz~2 MHz under visible light irradiation. The samples coated fluoride tin oxide glass (FTO) electrode, graphite sheet and Ag/AgCl electrode were used as working electrode, counter electrode and reference electrode. The samples coated fluoride tin oxide glass (FTO) electrode was prepared as follows: The FTO was previously cleaned by sonication in the solution with a sequence as acetone, ethanol and water. After that, the samples and $Mg(NO_3)_2$ were dispersed in isopropanol solution with concentration of 1 g L^{-1} and 0.05 g L^{-1}, respectively. The samples were finally deposited on FTO via an electrophoresis process under 10 V for 2 min. The photocurrent-time measurement was performed with a three-electrode system as that in EIS measurement. During the visible-light on and off over time, the transient photocurrent was obtained in 0.1 M Na_2SO_4 solution (O_2-saturated) at applied voltage of 0 V.

1.12. Femtosecond transient absorption spectroscopic measurement

Femtosecond transient absorption spectroscopic measurement was conducted using a Yb:KGW laser (Pharos, Light Conversion Ltd., Lietuvos). The

wavelength of fundamental output was at 1030 nm. For generation of 400 nm pump pulses, the second harmonic of 2HNOPA (Orpheus-N-2H, Light Conversion Ltd. Lietuvos) with output length at 800 nm was used. The probe pulses were generated through supercontinuum, where a small fraction of the fundamental 1030 nm laser was focused into a sapphire plate for visible detection, or a small fraction of the SHG of 1030 nm was focused into a CaF_2 plate for near UV detection. Time delay between the pump and probe pulses was controlled by a delay line. The fs-TA signals were measured using the commercial TA100 system. The pulse-to-pulse spectral analysis was conducted at 10 kHz for the visible detection. The signal-to-noise ratio (ΔO.D.) was better than 1×10^{-5} after averaging 5000 pump-on and pump-off shots for each data point.

1.13. Electrochemical measurement of ORR and WOR

The number of transferred electrons of photocatalyst in oxygen reduction reaction (ORR) was measured through rotating disk electrode (RDE) measurements, which were performed on a Pine AFMSRXE electrochemical system (UK) with a CHI760E electrochemical workstation (Chenhua, China) by a three-electrode configuration test cell. In the three-electrode setup, the samples coated glassy carbon electrode, Hg/HgCl electrode and graphite rod were used as working electrode, reference electrode and counter electrode. The preparation of sample coated glassy carbon electrode was based on the following process: 2.5 mg samples were dispersed in a mixture solution of 985 μL of ultrapure water, 15 μL of isopropanol and 15 μL of Nafion solution (5 wt.%). Then catalyst slurry was drop-added on the surface of glassy carbon electrode and dried at room temperature under natural air. The linear sweep voltammograms (LSV) were performed in O_2-saturated phosphate buffer solution (concentration of 0.1 mol L^-

^{1}, pH = 7) with the rotation speeds at 400 rpm, 900 rpm, 1200 rpm and 1600 rpm. The Koutecky-Levich (K-L) equations are as follows[9,10]:

$$J^{-1} = J_k^{-1} + B^{-1}\omega^{-1/2} \quad \text{Equation (S5)}$$

$$B = 0.2nF\nu^{-1/6}CD^{2/3} \quad \text{Equation (S6)}$$

Where J is current density, J_k is kinetic current density, ω is rotating speed (rpm), F is Faraday constant (96485 C mol^{-1}), ν is kinetic viscosity of water (0.01 cm^2 s^{-1}), C is bulk concentration of O_2 in water (1.26×10^{-3} mol cm^{-3}), and D is diffusion coefficient of O_2 (2.7×10^{-5} cm^2 s^{-1}).

Rotating ring disk electrode (RRDE) test was also conducted to study ORR and water oxidation reaction (WOR) with sample coated electrode as working electrode. The LSV polarization curves of ORR and WOR were recorded in 0.1 mol L^{-1} phosphate buffer solution (pH = 7) with sweep rate of 10 mV s^{-1} at 1000 rpm. For the ORR measurement in an O_2-saturated solution, potential range on disk electrode was set to -1~0 V vs Ag/AgCl and the fixing potential on ring electrode as 0.75 V vs Ag/AgCl. During WOR measurement, the potential on disk electrode ranged from 1.0 V to 2.1 V and the potential on ring electrode was set as -0.25 V vs Ag/AgCl and 0.75 V vs Ag/AgCl to measure O_2 and H_2O_2 production in an Ar atmosphere.

1.14. Electron paramagnetic resonance measurement

The electron paramagnetic resonance was conducted to detect superoxide radical or hydroxide radical with addition of DMPO as spin-trapping reagent and singlet oxygen with addition of TEMP as spin-trapping reagent. The photocatalyst was dispersed in ultrapure water for detection of hydroxide radical and singlet oxygen and in MeOH for detection of superoxide radical in a Pyrex glass sealed with rubber septum cap under visible light irradiation.

293 **1.15. Colorimetric detection of $\cdot O_2^-$ by NBT method**

294 Ni-CDs/COFs was dispersed in NBT aqueous solution and the suspension
295 was stirred in the dark for 20 min. After light irradiation, 2.5 mL sample was
296 taken out and filtrated through a 0.22 μm PES filter to remove photocatalyst. The
297 absorbance of samples was measured via a UV-vis spectrophotometer.

298 **1.16. Isotope labelling experiment**

299 1 mg Ni-CDs/COFs was dispersed in 1 mL $H_2{}^{18}O$. Then 1 mg $NaIO_4$ was
300 added as electron scavenger. The air was then evacuated and Ar was flowed into
301 the reactor. Mixture was further exposed to light source for 2 h. The gas products
302 were analyzed using GC-MS. After that, MnO_2 was added into solution and
303 reactor was sealed again. The mixture was sonicated for 5 min, and the resulting
304 gas productors were analyzed again through GC-MS.

305 **1.17. Cefalexin and orange II degradation through Fenton reaction**

306 The cefalexin aqueous solution with concentration of 10 mg L^{-1} and orange
307 II aqueous solution with concentration of 25 mg L^{-1} were firstly prepared. Then,
308 5 mL filtered photocatalytic reaction solution and 95 mL above cefalexin solution
309 or orange II solution were uniformly mixed before adding 1.5 mg $FeSO_4$. During
310 the Fenton reaction, 3 mL of sample was taken out every 3 min in cefalexin
311 degradation and every 2 min in orange II degradation with quick addition of 20
312 μL isopropanol. The content of orange II was detected at 486 nm by a UV-vis
313 spectrophotometer. The concentration of cefalexin was measured by a Waters
314 2695 high performance liquid chromatography (HPLC; USA).

315 **1.18. Computational methods**

316 The density functional theoretical calculation was performed through the
317 density functional theory (DFT) by the Gaussian 09W. The geometry

optimization was carried out using B3LYP with 6-31G (d) basis sets. The lowest unoccupied molecular orbitals (LUMO) and highest occupied molecular orbitals (HOMO) are calculated based on optimized structure and analyzed by Multiwfn 3.8 softare.[11,12] High accuracy energies were calculated by using the 6-311G (d) basis sets. The reaction free energy as ΔG was calculated according to the equation (S7).[13,14]

$$\Delta G = \Delta E + \Delta ZPE - T\Delta S \qquad \text{Equation (S7)}$$

Where ΔE is the energy change between reactants and intermediates, ZPE is the zero-point energy, T is the temperature set as 298.15 K, S is the entropy energy.

2. Supplementary Figures and Tables

2.1. SEM images of COFs and Ni-CDs/COFs

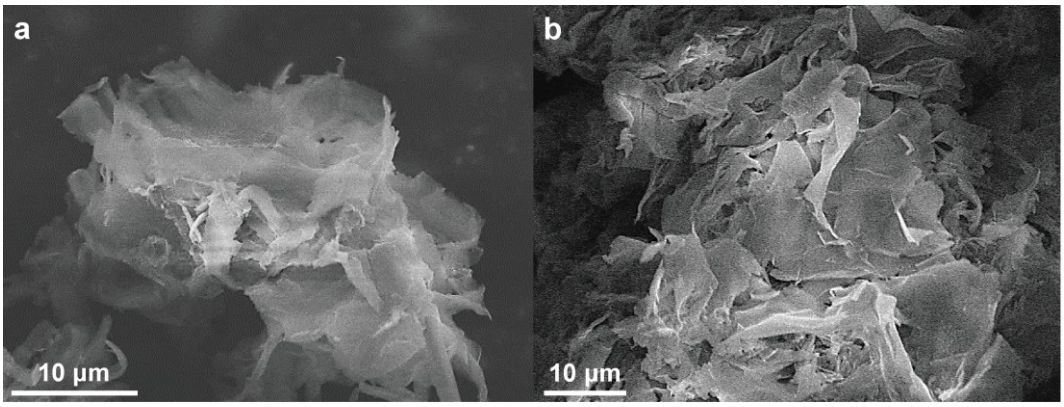

Fig. S1 SEM images of (a) COFs and (b) Ni-CDs/COFs.

2.2. TEM image of Ni-CDs

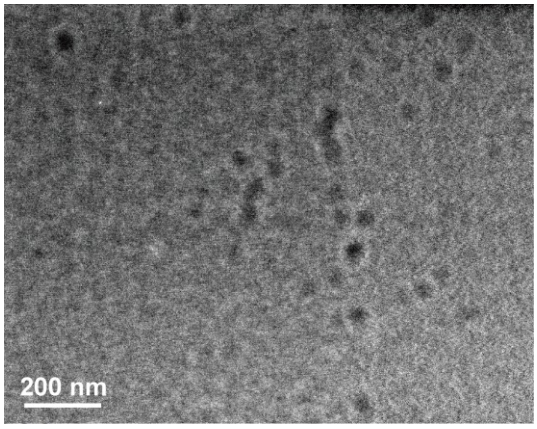

Fig. S2 TEM image of Ni-CDs.

2.3. HADDF-STEM image of Ni-CDs

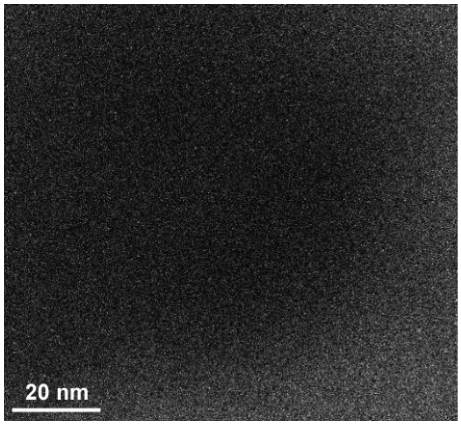

Fig. S3 HADDF-STEM image of Ni-CDs.

2.4. XPS spectra of Ni-CDs/COFs, Ni-CDs, O 1s and N 1s of Ni-CDs

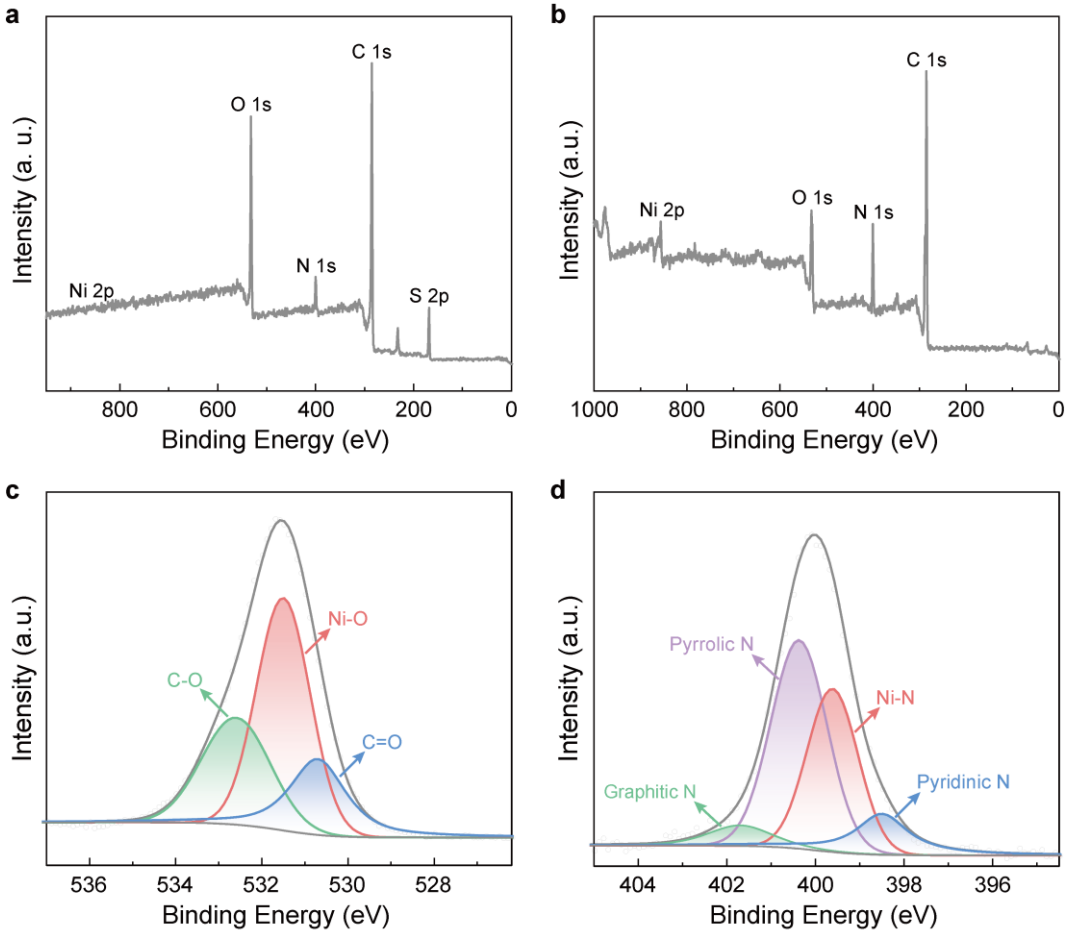

Fig. S4 XPS spectra of (a) Ni-CDs/COFs and (b) Ni-CDs. High-resolution XPS spectra of (c) O 1s and (d) N 1s in Ni-CDs.

2.5. Elemental content measured by XPS

Table S1 XPS elemental content of Ni-CDs.

Element	Content (wt.%)
Carbon	60.30
Nickel	10.54
Nitrogen	10.31
Oxygen	18.85

2.6. Content of Ni element measured by ICP

Table S2 ICP result of Ni content in Ni-CDs.

Element	Content (wt.%)
Nickel	10.25

2.7. Ni K-edge EXAFS fitting curves of Ni-foil, NiO, Ni_2O_3, NiPc and Ni-CDs in k-space

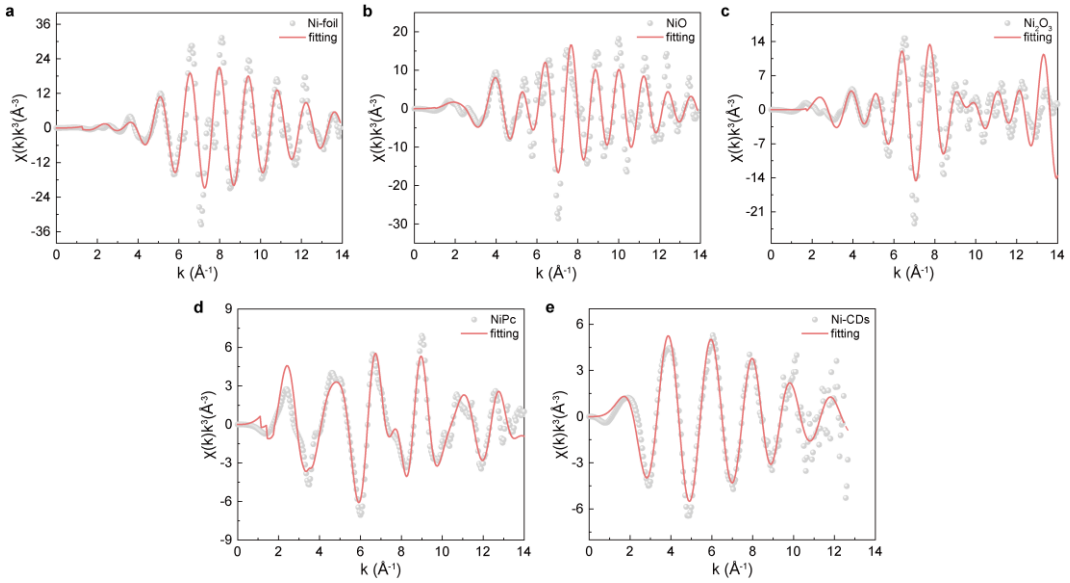

Fig. S5 Ni K-edge EXAFS fitting curves of (a) Ni-foil, (b) NiO, (c) Ni_2O_3, (d) NiPc and (e) Ni-CDs in k-space.

2.8. FT-EXAFS curves at R-space for Ni K-edge of Ni-foil, NiO, Ni_2O_3 and NiPc

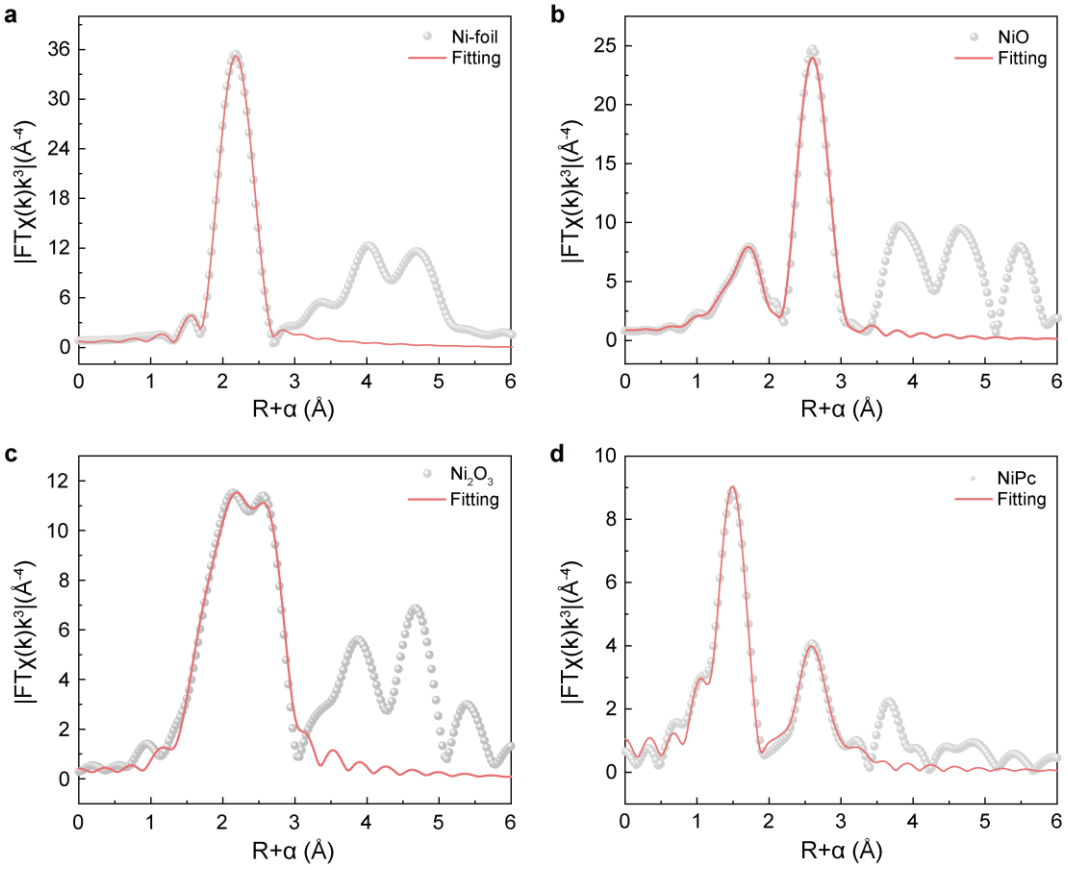

Fig. S6 FT-EXAFS curves at R-space for Ni K-edge of (a) Ni-foil, (b) NiO, (c) Ni_2O_3 and (d) NiPc.

2.9. EXAFS fitting parameters for Ni K-edge of Ni-CDs, standard Ni-foil, NiO, Ni_2O_3 and NiPc

Table S3 EXAFS fitting parameters for Ni K-edge of Ni-CDs, standard Ni-foil, NiO, Ni_2O_3 and NiPc.

Sample	Shell	C.N.	R (Å)	σ^2 (Å^2)	ΔE_0 (eV)	*R* factor
Ni-foil	Ni-Ni	12.0	2.486±0.002	0.0063±0.0003	6.3±0.4	0.0013
NiO	Ni-O	6.0±0.7	2.094±0.001	0.0071±0.0017	4.0±0.6	0.0052
	Ni-Ni	12.3±0.9	2.948±0.001	0.0069±0.0006	0.7±0.3	
Ni_2O_3	Ni-O	3.8±0.5	2.103±0.001	0.0009±0.0014	11.3±0.7	0.0049
	Ni-Ni	7.4±1.0	2.773±0.001	0.0018±0.0012	-12.2±0.5	
NiPc	Ni-N	4.0±0.2	1.890±0.001	0.0030±0.0007	4.8±0.4	0.0039
	Ni-C	7.8±1.5	2.935±0.001	0.0039±0.0018	7.6±0.7	
Ni-CDs	Ni-N	2.9±0.1	2.003±0.001	0.0010±0.0004	11.9±1.1	0.0005
	Ni-O	1.1±0.1	2.113±0.003		-3.4±0.2	

C.N., coordination numbers; R, interatomic distance; σ^2, Debye-Waller factors; ΔE_0, inner potential correction; R factor, goodness of fit; S_0^2 was fixed to 0.807 as determined from Ni foil fitting.

2.10. Optimization of ratio of Ni-CDs and COFs

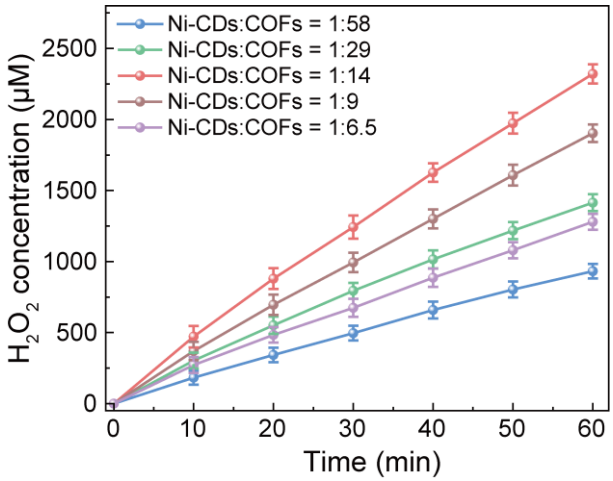

Fig. S7 Optimization of ratio of Ni-CDs and COFs.

2.11. Time-dependent photocatalytic H_2O_2 production by Ni-CDs and Ni-CDs/COFs in pure water

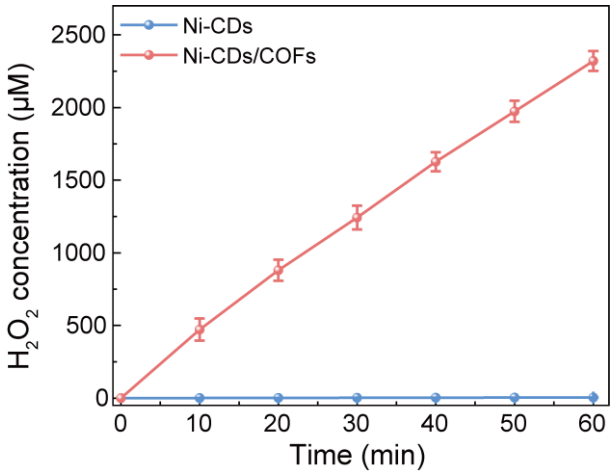

Fig. S8 Time dependent photocatalytic H_2O_2 production by Ni-CDs and Ni-CDs/COFs in pure water.

2.12. Composition of yield, AQY and SCC efficiency of various photocatalytic system in H_2O_2 production

Table S4 Comparison of yield, AQY and SCC efficiency of various photocatalytic system in H_2O_2 production.

Catalyst	Solution and concentration	Light Source	Formed H_2O_2 ($\mu mol\ h^{-1}\ g^{-1}$)	AQY (%)	SCC (%)	Ref.
Ni-CDs/COFs	Pure water, 0.2 g L^{-1}	$\lambda \geq 420$ nm	11603	20.4 (420 nm)	1.56	This work
PI-BD-TPB	Pure water, 0.75 g L^{-1}	Xe-lamp	3777.3	14.28 (420 nm)	0.92	15
Kf-AQ	Pure water, 0.17 g L^{-1}	$\lambda > 400$ nm	4784	15.8 (400 nm)	0.7	16
TTF@Por-COF-cya	Pure water, 0.1 g L^{-1}	$\lambda > 420$ nm	6994	14.98 (420 nm)	N. T.	17
Ca(II)@ACG	Pure water, 0.2 g L^{-1}	$\lambda > 420$ nm	1021.5	3.12 (420 nm)	N. T.	18
o-COF-TpPzda	Pure water, 0.125 g L-1	$\lambda > 420$ nm	4396	N. T.	0.46	19
Hz-TP-BT-COF	Pure water, 0.2 g L^{-1}	$\lambda \geq 420$ nm	5700	17.5 (420 nm)	N. T.	20
C_5N_2	Pure water, 1 g L^{-1}	Xe-lamp	1343.6	N. T.	0.26	21
FS-COFs	Pure water, 0.4 g L^{-1}	$\lambda \geq 420$ nm	3904.2	6.21 (420 nm)	N. T.	22
TAPT-FTPB COFs	Pure water, 1 g L^{-1}	Xe-lamp	3780	N. T.	1.22	23
TPT-Cz-phCN	Pure water, 0.02 g L^{-1}	$\lambda \geq 400$ nm	2534	19.1 (420 nm)	0.64	24

398

Catalyst	Solution and concentration	Light Source	Formed H_2O_2 ($\mu mol\ h^{-1}\ g^{-1}$)	AQY (%)	SCC (%)	Ref.
20COFIS	Pure water, 0.17 g L^{-1}	Xe-lamp	5713.2	0.55 (420 nm)	N. T.	25
SA-TCPP	Pure Water, 1.5 g L^{-1}	$\lambda \geq 400$ nm	440	14.9 (420 nm)	0.6	3
TTF-BT-COF	Pure water, 0.5 g L^{-1}	Xe-lamp	6900	11.2 (420 nm)	0.49	26
TP-$DPBD_{30}$-COF	Pure water, 0.17 g L^{-1}	$\lambda \geq 420$ nm	7200	18 (420 nm)	0.91	27
CTF-NSs	Pure water, 0.1 g L^{-1}	$\lambda > 420$nm	5007	16.8 (420 nm)	0.91	28
CNW03	Pure water, 0.1 g L^{-1}	$\lambda \geq 420$ nm	556	8.53 (420 nm)	0.31	29
Ni_{SAPs}-PuCN	Pure water 1 g L^{-1}	$\lambda \geq 420$ nm	342.2	10.9 (420 nm)	1.17	30
g-COF-DMDP-2	Pure water, 0.25 g L^{-1}	$\lambda > 420$nm	3820	1.83 (420 m)	N. T.	31
S_v-ZIS	Pure water, 0.67 g L^{-1}	$\lambda \geq 400$ nm	1706.4	9.9 (420 nm)	0.81	32
Hf-PMOF/APF	Pure water 0.2 g L^{-1}	Xe-lamp	2995.1	4.53 (420 nm)	N. T.	33
CN-PDA	Pure water, 1.5 g L^{-1}	$\lambda \geq 400$ nm	495.2	5.1 (400 nm)	0.14	34
DMCR-1NH	Pure water, 0.46 g L^{-1}	$\lambda > 420$ nm	2588	10.1 (420 nm)	N. T.	35
TACOF-1-COOH	Pure water, 0.14 g L^{-1}	$\lambda > 420$ nm	3542	5.7 (420 nm)	0.55	36
CoO_x-BCN-FeOOH	Pure water, 1 g L^{-1}	$\lambda \geq 420$nm	340	8.36% (420 nm)	0.95	37

399

2.13. H_2O_2 yield of various photocatalysts with sacrificial agent

Table S5 H_2O_2 yield of various photocatalysts with sacrificial agent.

Catalyst	Concentration	Solution	Light source	Formed H_2O_2 ($\mu mol\ h^{-1}\ g^{-1}$)	Ref.
CN-KI_3-KI-MV	0.5 g L^{-1}	Isopropanol (10 vol%) in water	$\lambda \geq 420nm$	46400	38
TiO_2/MoS_x-Au	0.1 g L^{-1}	Ethanol (10 vol %) in water	Xe-lamp	30440	39
PAF-363	0.02 g L^{-1}	Ethanol (10 vol %) in water	$\lambda > 420$ nm	11733	40
JNM-25	0.6 g L^{-1}	Isopropanol (10 vol%) in water	Xe-lamp	17476	41
TFPA-TAPT-COF-Q	0.5 g L^{-1}	Benzyl alcohol (10%) in water	Xe-lamp	11832	42
CN-KCl/KI	0.2 g L^{-1}	Isopropanol (10 vol%) in water	$\lambda > 420$ nm	13100	2
KDBT-A	0.17 g L^{-1}	Methanol (10 vol%) in water	Xe-lamp	11286	43
CNW03	0.1 g L^{-1}	Isopropanol (10%) in water	$\lambda \geq 420nm$	15882	29
PMCR-1	0.45 g L^{-1}	Isopropanol (9 vol%) in water	$\lambda \geq 400nm$	5500	44
Pylm-COF	0.2 g L^{-1}	Benzyl alcohol (10%) in water	$\lambda > 420$ nm	7600	45
TpAP[5]	0.08 g L^{-1}	Ethanol (10 vol%) in water	$\lambda \geq 420nm$	2343	46
Fl-CN	0.5 g L^{-1}	Ethanol (10 vol %) in water	$\lambda \geq 420nm$	1893	47
P2ZIS	0.1 g L^{-1}	Isopropanol (10 vol%) in water	$\lambda \geq 420nm$	2107.7	48

2.14. Cyclic photocatalytic production of H_2O_2 by Ni-CDs/COFs

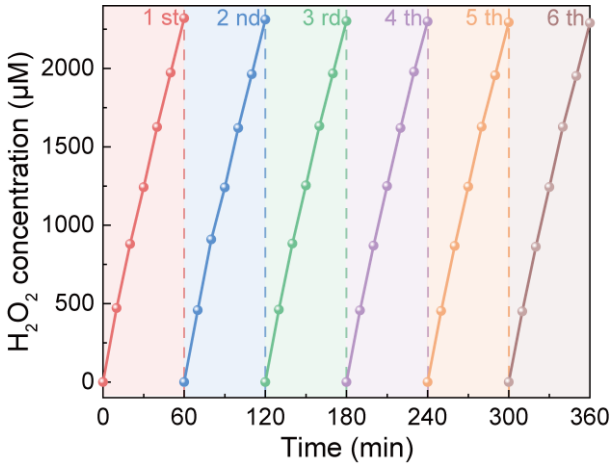

Fig. S9 Cyclic photocatalytic production of H_2O_2 by Ni-CDs/COFs in pure water.

2.15. SEM image of Ni-CDs/COFs after photocatalytic H_2O_2 production

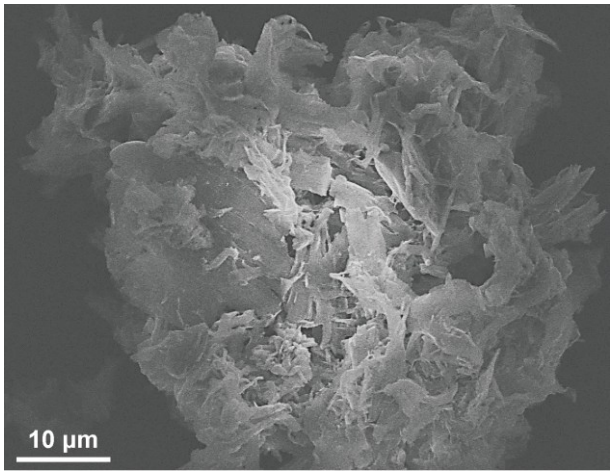

Fig. S10 SEM image of Ni-CDs/COFs after photocatalytic H_2O_2 production.

2.16. XRD pattern of Ni-CDs/COFs after photocatalytic H_2O_2 production

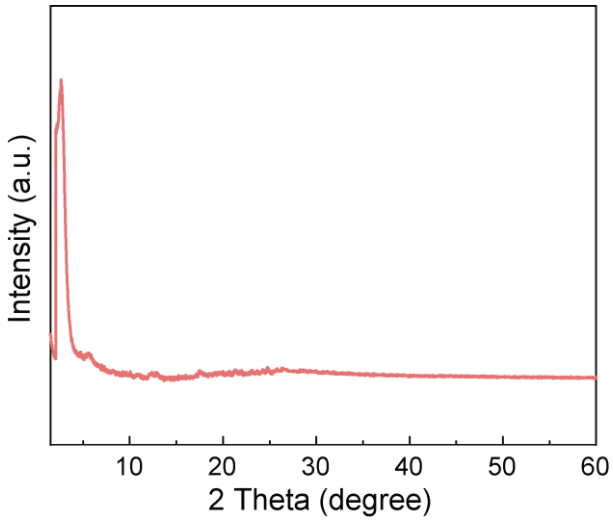

Fig. S11 XRD pattern of Ni-CDs/COFs after photocatalytic H_2O_2 production.

2.17. FT-IR spectrum of Ni-CDs/COFs after photocatalytic H_2O_2 production

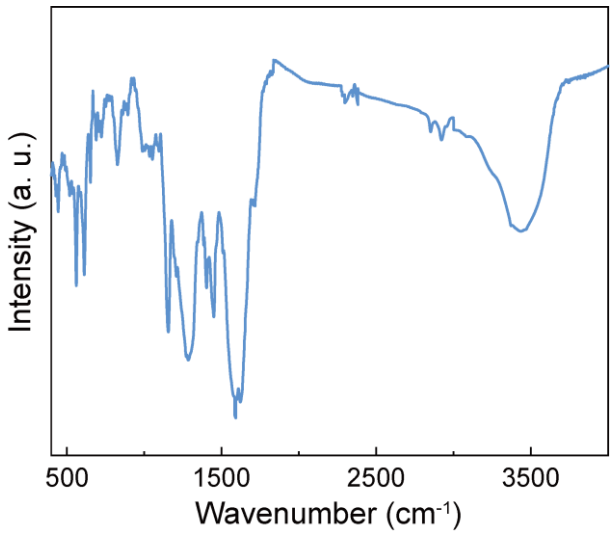

Fig. S12 FT-IR spectrum of Ni-CDs/COFs after photocatalytic H_2O_2 production.

2.18. Photocatalytic H_2O_2 production by Ni-CDs/COFs after storage for 4 weeks

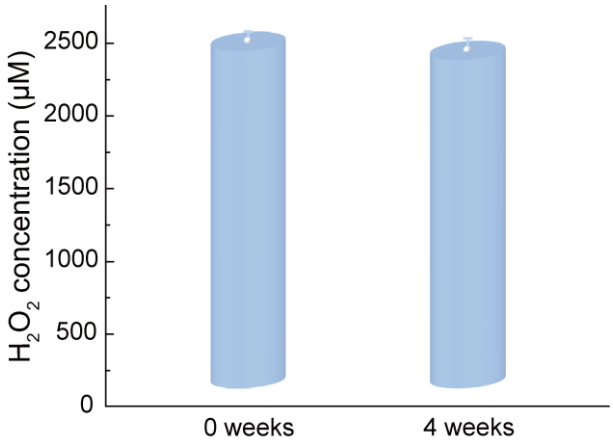

Fig. S13 Photocatalytic H_2O_2 production by Ni-CDs/COFs after storage for 4 weeks.

2.19. Photocatalytic H_2O_2 decomposition under light irradiation

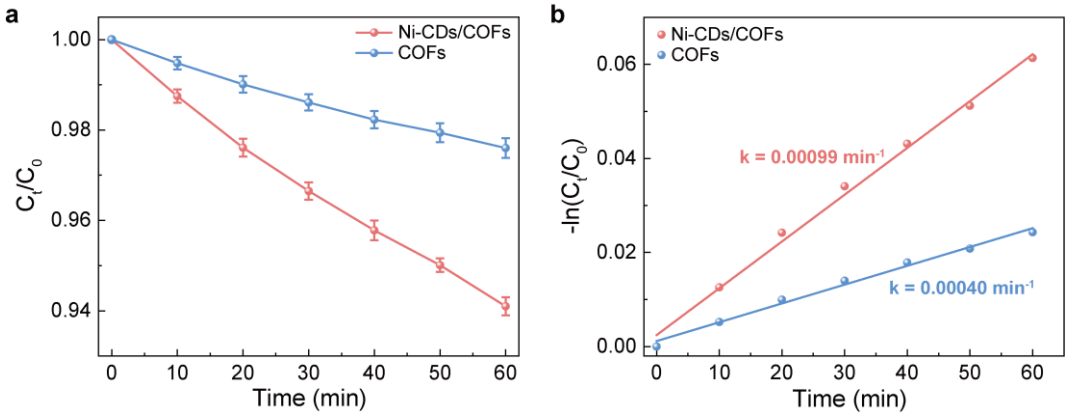

Fig. S14 (a) Photocatalytic decomposition of H_2O_2 under light irradiation. (b) Pseudo first order kinetic fitting curves of photocatalytic H_2O_2 decomposition process.

2.20. Degradation of Orange II and cefalexin

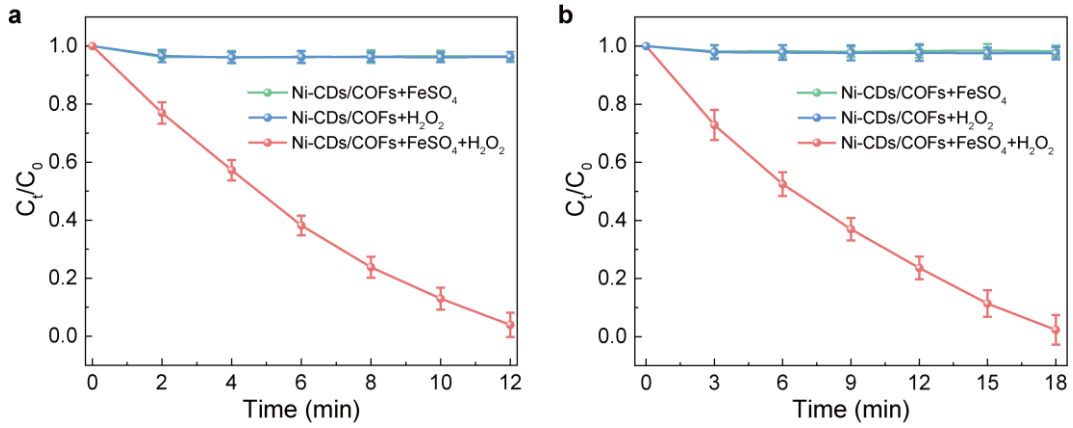

Fig. S15 Degradation of (a) Orange II (25 mg L^{-1}) and (b) cefalexin (10 mg L^{-1}).

2.21. H_2O_2 yield of various immobilized photocatalysts

Table S6 H_2O_2 yield of various immobilized photocatalysts.

Photocatalyst	Solution	Formed H_2O_2 (μM cm^{-2} h^{-1})	Ref.
Ni-CDs/COFs	Pure water	57.2	This work
AmCOF	Pure water	4.8	49
Furan-BILP	Pure water	11.4	50
PI-BD-TPB	Pure water	0.1	15
OF-N32	Pure water	43.75	4
COF2-2CN	Pure water	0.044	51

2.22. UV-vis DRS spectrum of COFs

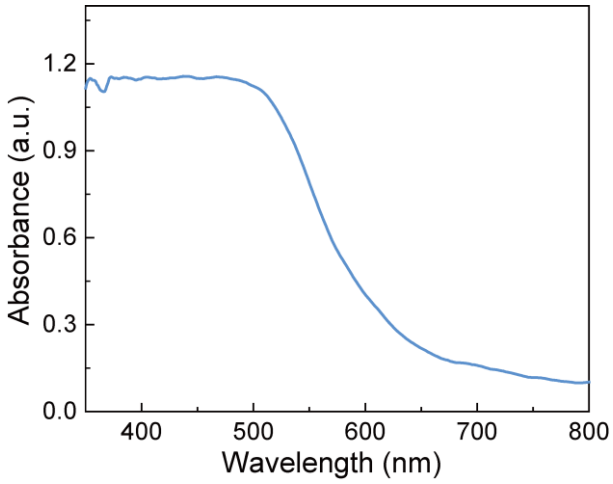

Fig. S16 UV-vis DRS spectrum of COFs.

2.23. Mott-Schottky plots of COFs and Ni-CDs/COFs

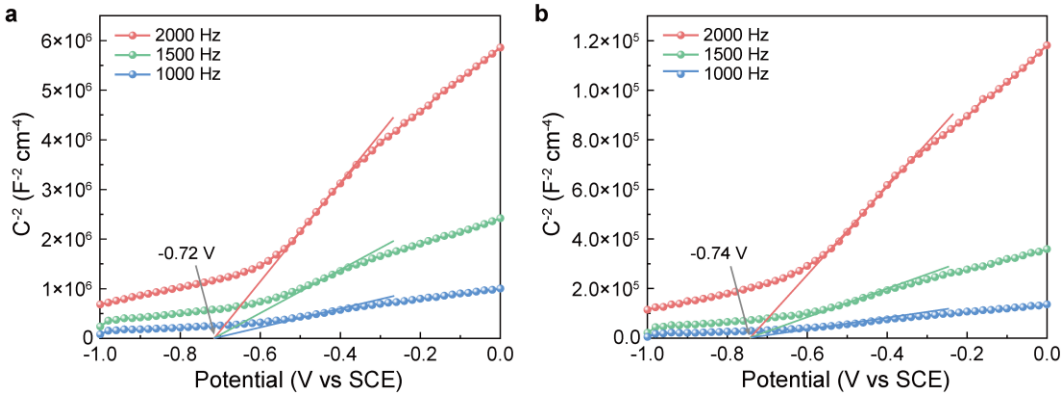

Fig. S17 Mott-Schottky plots of (a) COFs and (b) Ni-CDs/COFs.

2.24. VB XPS spectra of COFs and Ni-CDs/COFs

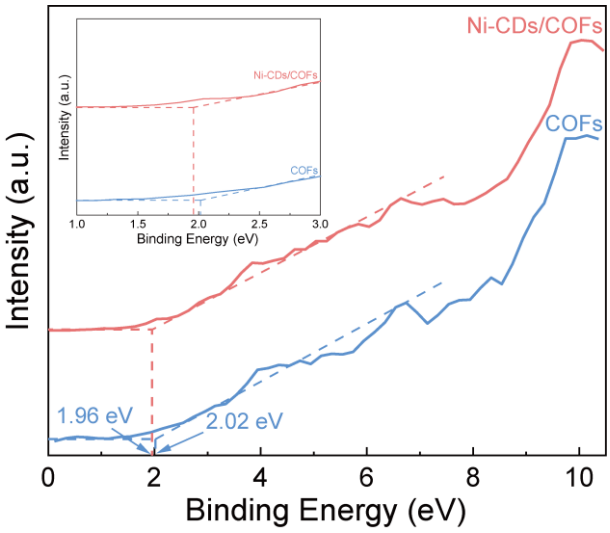

Fig. S18 VB XPS spectra of COFs and Ni-CDs/COFs.

2.25. LUMO and HOMO of COFs

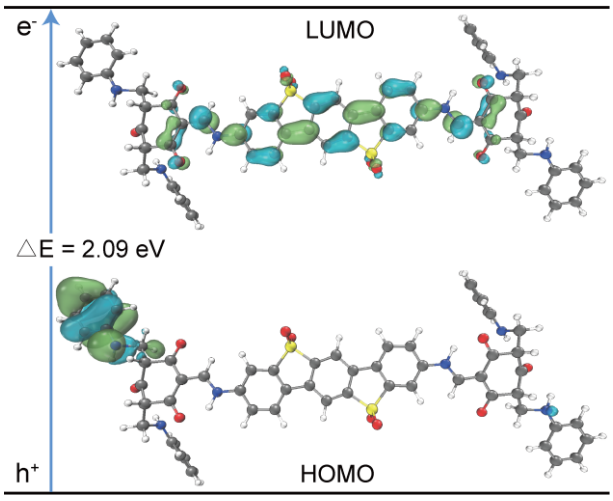

Fig. S19 LUMO and HOMO of COFs.

2.26. SEM image, XRD pattern and FT-IR spectrum of CDs/COFs

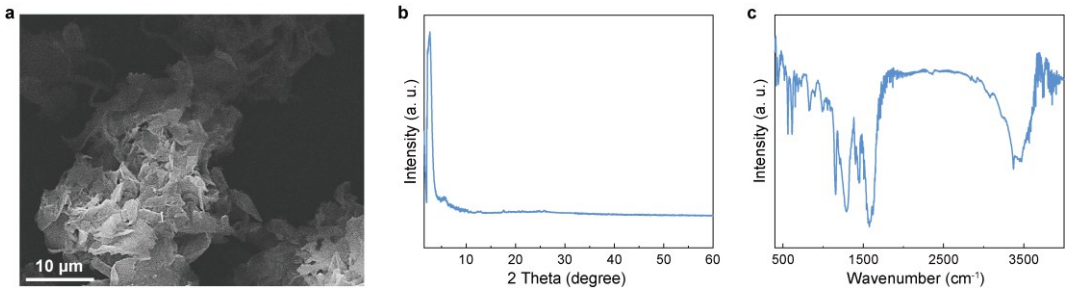

Fig. S20 (a) SEM image, (b) XRD pattern and (c) FT-IR spectrum of CDs/COFs.

2.27. EIS spectra and Bode-phase plots of COFs, CDs/COFs and Ni-CDs/COFs

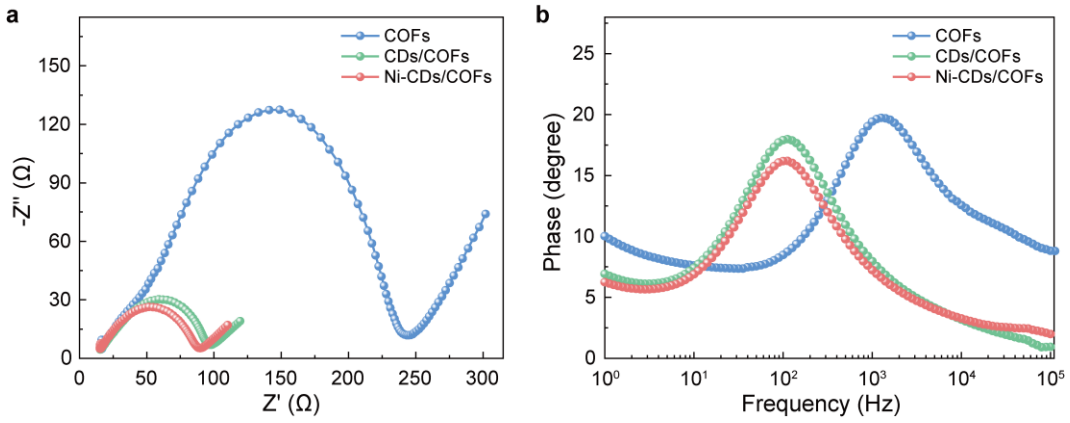

Fig. S21 (a) EIS spectra and (b) Bode-phase plots of COFs, CDs/COFs and Ni-CDs/COFs.

2.28. Photocurrent of COFs, CDs/COFs and Ni-CDs/COFs

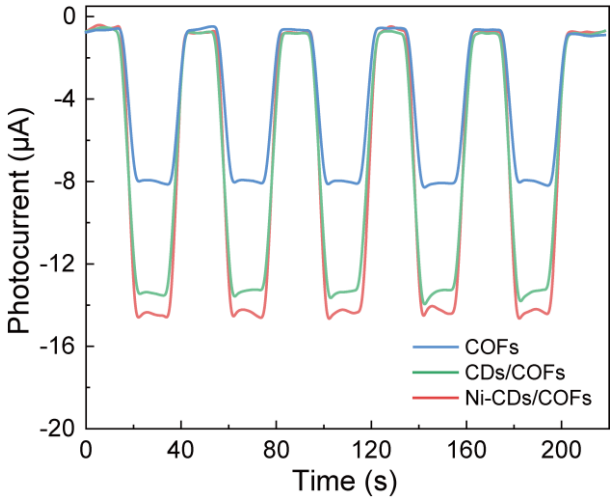

Fig. S22 Photocurrent of COFs, CDs/COFs, and Ni-CDs/COFs.

2.29. fs-TA spectra of COFs, CDs/COFs and Ni-CDs/COFs probed at different time delays

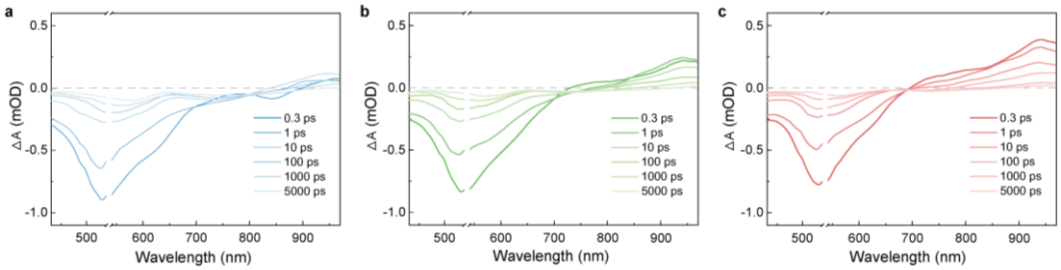

Fig. S23 fs-TA spectra of (a) COFs, (b) CDs/COFs and Ni-CDs/COFs probed at different time delays.

2.30. Normalized fs-TA decay dynamics of COFs, CDs/COFs and Ni-CDs/COFs probed at 530 nm

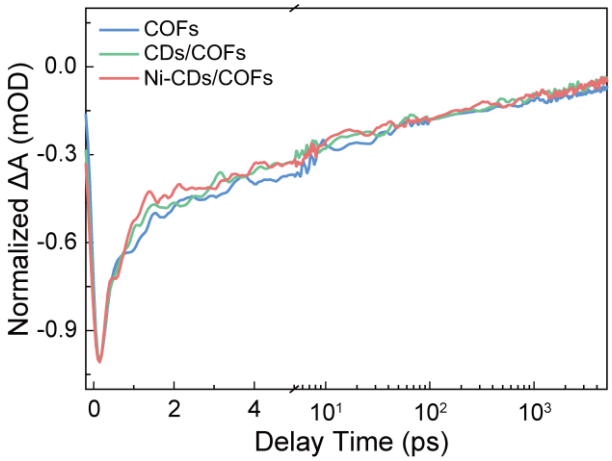

Fig. S24 Normalized fs-TA decay dynamics of COFs, CDs/COFs and Ni-CDs/COFs probed at 530 nm.

2.31. Time-dependent photocatalytic H_2O_2 production by CDs/COFs and CDs in pure water

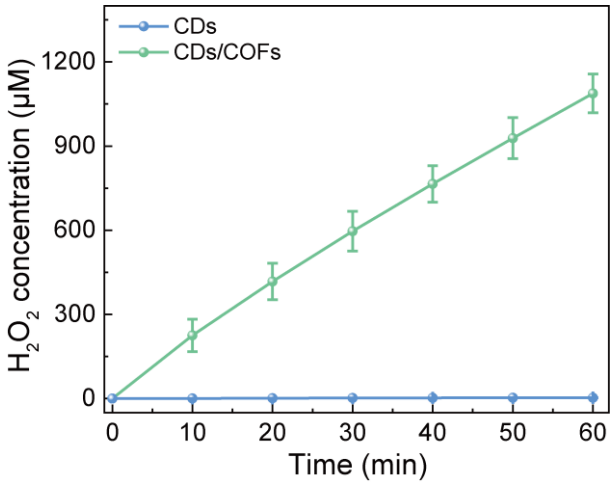

Fig. S25 Time-dependent photocatalytic H_2O_2 production by CDs/COFs and CDs in pure water.

2.32. Photocatalytic H_2O_2 production by Ni-CDs/COFs with different scavengers

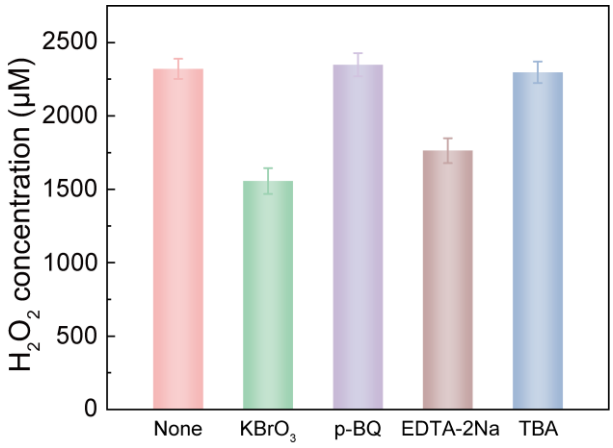

Fig. S26 Photocatalytic H_2O_2 production by Ni-CDs/COFs with different scavengers over one hour reaction.

2.33. LSV plots of COFs, CDs/COFs and Ni-CDs/COFs measured by RDE

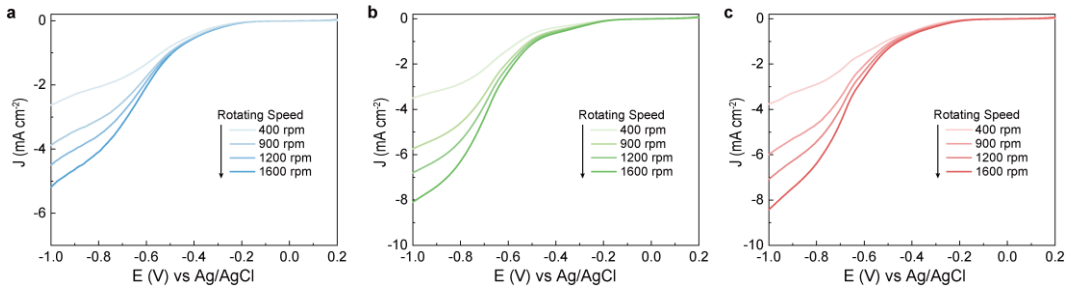

Fig. S27 LSV plots of (a) COFs, (b) CDs/COFs and (c) Ni-CDs/COFs measured by RDE.

2.34. RRDE measurement for H_2O_2 formation in ORR process

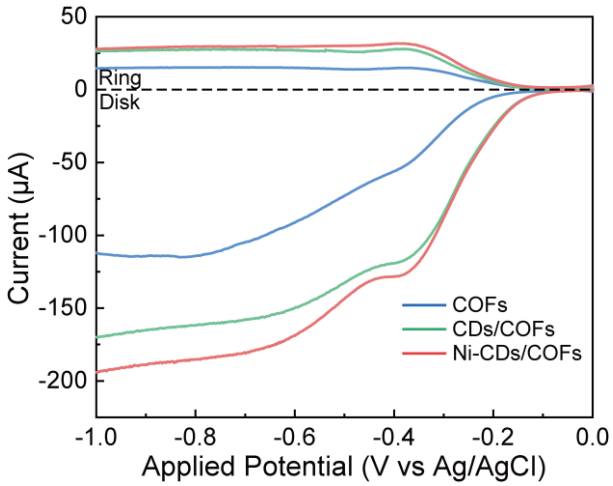

Fig. S28 RRDE voltammograms obtained in 0.1 mol L^{-1} phosphate buffer solution (disk electrode potential from -1 V vs Ag/AgCl to 0V vs Ag/AgCl, Pt ring electrode potential as 0.75 V vs Ag/AgCl to detect H_2O_2).

2.35. EPR spectra of $\cdot O_2^-$, $^1O_2$ and ·OH for Ni-CDs/COFs

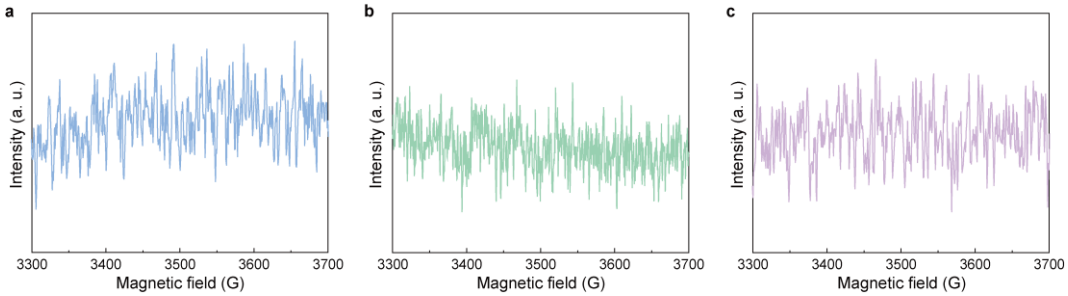

Fig. S29 EPR spectra of (a) $\cdot O_2^-$ (b) $^1O_2$ and (c) ·OH for Ni-CDs/COFs.

2.36. Detection of $\cdot O_2^-$ through NBT method

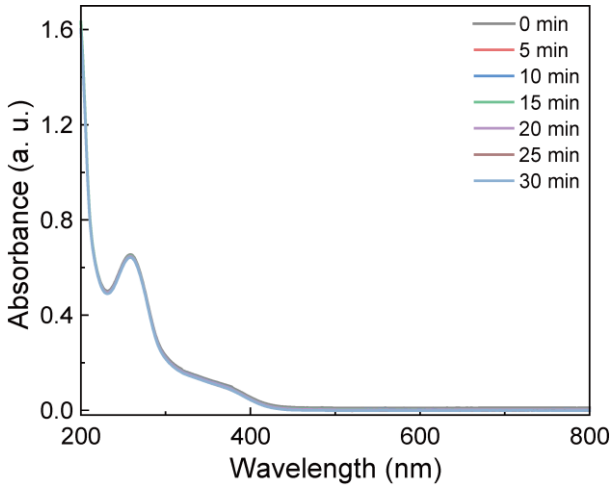

Fig. S30 Detection of $\cdot O_2^-$ through NBT method.

2.37. $H_2{}^{18}O$ isotope experiment to explore H_2O_2 evolution though WOR process

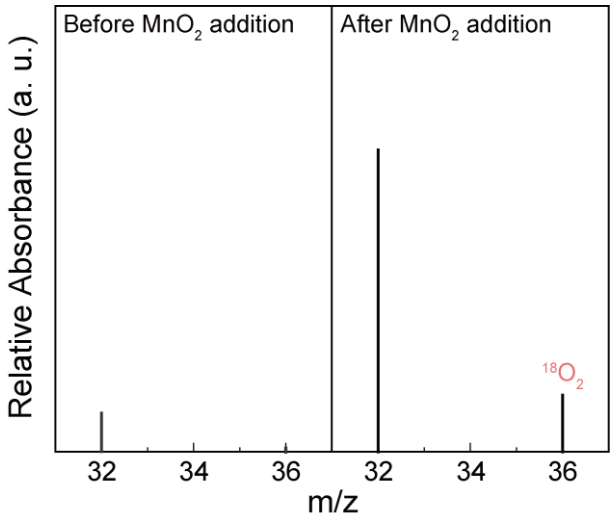

Fig. S31 $H_2{}^{18}O$ isotope experiment to explore H_2O_2 evolution though WOR process

2.38. RRDE measurement for O_2 formation in WOR process

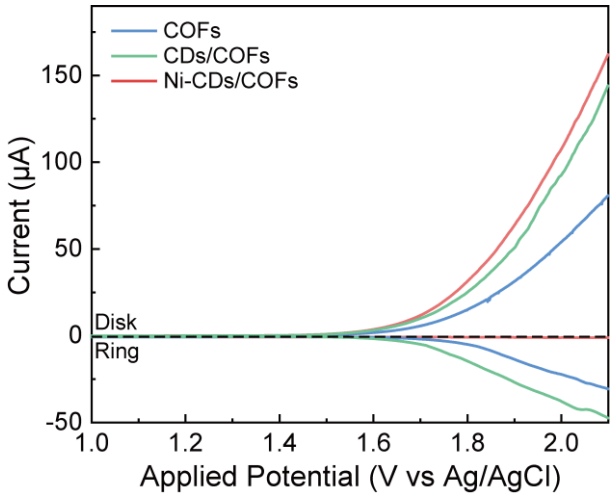

Fig. S32 RRDE voltammograms obtained in phosphate buffer solution (0.1 mol L^{-1}) (risk electrode potential from 1 V vs Ag/AgCl to 2.1 V vs Ag/AgCl, with Pt ring electrode potential as -0.25 V vs Ag/AgCl vs to detect O_2).

2.39. In-situ Raman spectra of Co-CDs/COFs and Mn-CDs/COFs in photocatalytic water oxidation

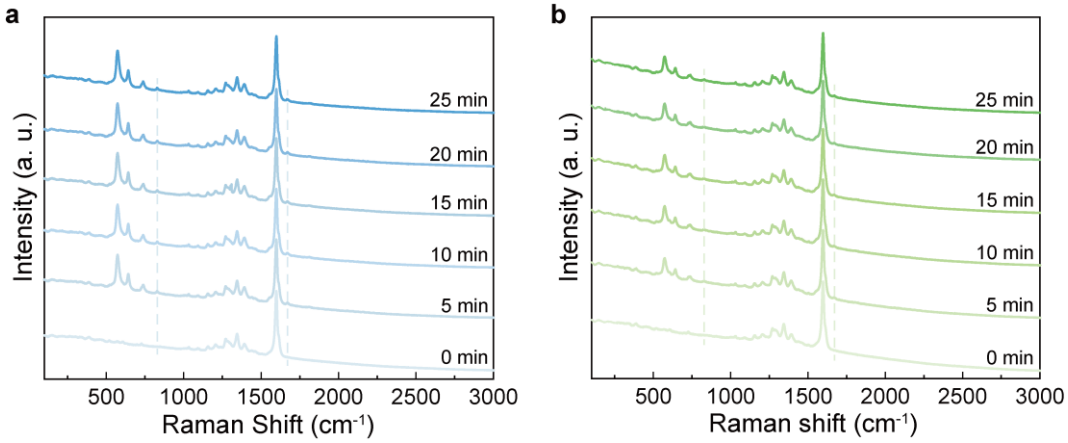

Fig. S33 In-situ Raman spectra of (a) Co-CDs/COFs and (b) Mn-CDs/COFs recorded in aqueous solution saturated with Ar under visible-light irradiation.

2.40. Photocatalytic H_2O_2 production by Co-CDs/COFs and Mn-CDs/COFs

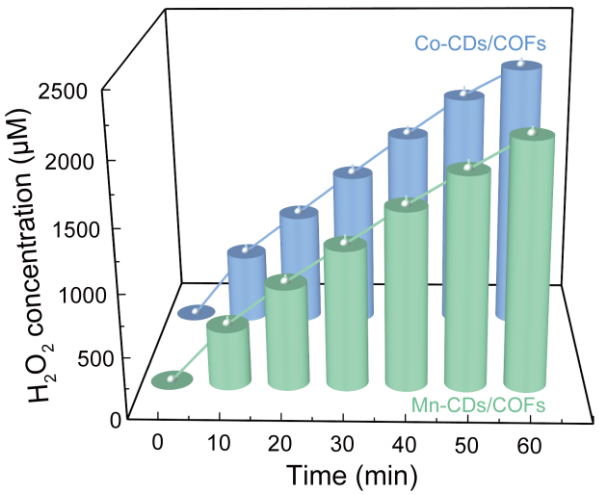

Fig. S34 Photocatalytic H_2O_2 production by Co-CDs/COFs and Mn-CDs/COFs (catalyst concentration as 0.2 g L^{-1}, pure water filled with O_2, $\lambda \geq 420$ nm, reaction temperature as 25 ℃).

2.41. Formation energy of O^* on carbon atom, O^* on nickel atom and OOH^* on carbon atom

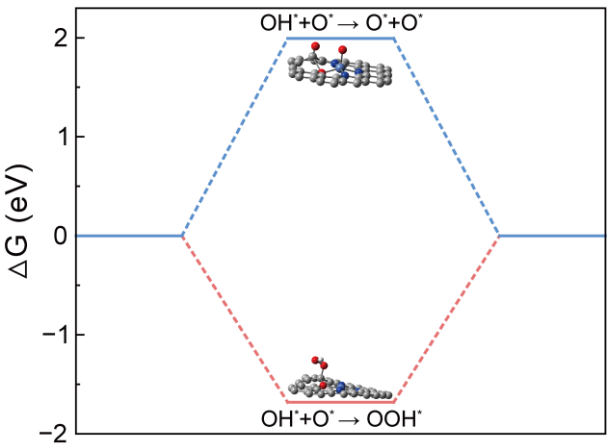

Fig. S35 Formation energy of O^* on carbon atom, O^* on nickel atom and OOH^* on carbon atom.

2.42. Formation energy of O_2 and H_2O_2 from OOH^*

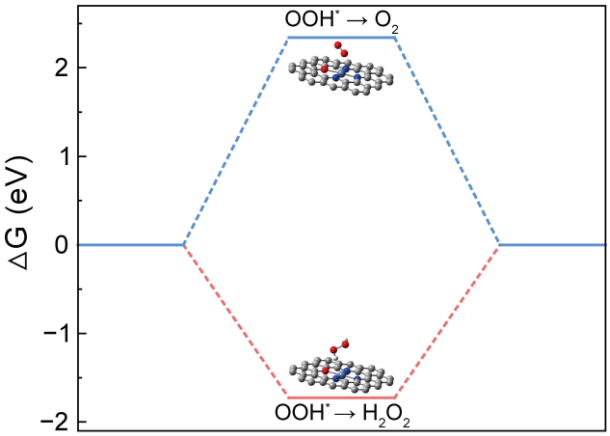

Fig. S36 Formation energy of O_2 and H_2O_2 from OOH^*.

2.43. Formation energy of OH^* on carbon atom, O^* on nickel atom and OH^* on nickel atom, O^* on carbon atom

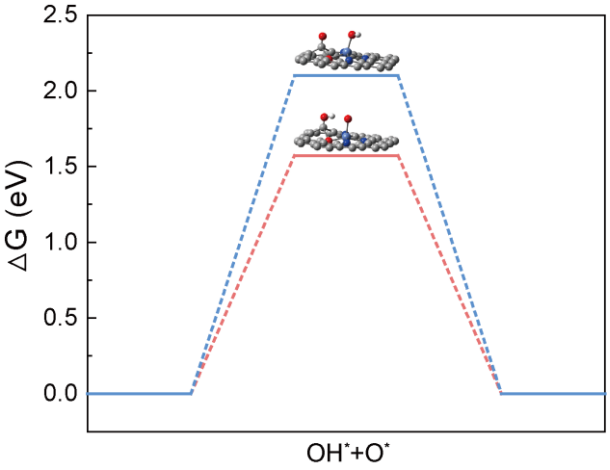

Fig. S37 Formation energy of OH^* on carbon atom, O^* on nickel atom and OH^* on nickel atom, O^* on carbon atom, respectively.

References

1 Y. Shiraishi, T. Takii, T. Hagi, S. Mori, Y. Kofuji, Y. Kitagawa, S. Tanaka, S. Ichikawa and T. Hirai, *Nat. Mater.*, 2019, **18**, 985-993.

2 L. Liu, F. Chen, J. Wu, J. Chen, H. Yu, *Proc. Natl. Acad. Sci. USA*, 2023, **120**, e2215305120.

3 Y. Zhang, C. Pan, G. Bian, J. Xu, Y. Dong, Y. Zhang, Y. Lou, W. Liu and Y. Zhu, *Nat. Energy*, 2023, **8**, 361-371.

4 F. Liu, P. Zhou, Y. Hou, H. Tan, Y. Liang, J. Liang, Q. Zhang, S. Guo, M. Tong and J. Ni, *Nat. Commun.*, 2023, **14**, 4344.

5 W. Ren, X. Tan, J. Qu, S. Li, J. Li, X. Liu, S. P. Ringer, J. M. Cairney, K. Wang, S. C. Smith, and C. Zhao, *Nat. Commun.* **2021**, *12*, 1449.

6 C. Wang, J. Zhang, K. Miao, M. Long, S. Lai, S. Zhao and X. Kang, *Adv. Mater.*, 2024, **36**, 2400433.

7 H. Xu, D. Cheng, D. Cao and X. Zeng, *Nat. Catal.*, 2024, **7**, 207-218.

8 H. Zhang, J. Gao, D. Raciti and A. Hall, *Nat. Catal.*, 2023, **6**, 807-817.

9 Z. Huang, S. Hu, M. Sun, Y. Xu, S. Liu, R. Ren, L. Zhuang, T. Chan, Z. Hu, T. Ding, J. Zhou, L. Liu, M. Wang, Y. Huang, N. Tian, L. Bu, L. Huang and X. Huang, *Nat. Commun.*, 2024, **15**, 1097.

10 L. Shang, Y. Ni, Y. Wang, W. Yang, L. Wang, H. Li, K. Zhang, Z. Yan and J. Chen, *Adv. Mater.*, 2024, **36**, 2413141.

11 T. Lu and F. Chen, *J. Comput. Chem.*, 2011, **33**, 580-592.

12 J. Zhang and T. Lu, *Phy. Chem. Chem. Phy.*, 2021, **23**, 20323-20328.

13 R. Wu, Q. Meng, J. Yan, Z. Zhang, B. Chen, H. Liu, J. Tai, G. Zhang, L. Zheng, J. Zhang and B. Han, *Nat. Catal.*, 2024, **7**, 702-718.

14 X. Zheng, J. Yang, P. Li, Q. Wang, J. Wu, E. Zhang, S. Chen, Z. Zhuang, W. Lai, S. Dou, W. Sun, D. Wang and Y. Li, *Sci. Adv.*, 2023, **9**, eadi8025.

15 W. Chi, Y. Dong, B. Liu, C. Pan, J. Zhang, H. Zhao, Y. Zhu and Z. Liu, *Nat. Commun.*, 2024, **15**, 5316.

16 X. Zhang, S. Cheng, C. Chen, X. Wen, J. Miao, B. Zhou, M. Long and L. Zhang, *Nat. Commun.*, 2024, **15**, 2649.

17 Z. Gong, Y. Gao, J. Li, Z. Cai, N. Liu and J. Jiang, *Angew. Chem. Int. Ed.*, 2025, **137**, e202423205.

18 C. He, J. Lei, X. Li, Z. Shen, L. Wang and J. Zhang, *Angew. Chem. Int. Ed.*, 2024, **63**, e202406143.

19 T. Yang, D. Zhang, A. Kong, Y. Zou, L. Yuan, C. Liu, S. Luo, G. Wei and C. Yu, *Angew. Chem. Int. Ed.*, 2024, **136**, e202404077.

20 R. Liu, Y. Chen, H. Yu, M. Položij, Y. Guo, T. C. Sum, T. Heine and D. Jiang, *Nat. Catal.* 2024, **7**, 195-206.

21 J. Ma, C. Peng, X. Peng, S. Liang, Z. Zhou, K. Wu, R. Chen, S. Liu, Y. Shen, H. Ma and Y. Zhang, *J. Am. Chem. Soc.*, 2024, **146**, 21147-21159.

22 Y. Luo, B. Zhang, C. Liu, D. Xia, X. Ou, Y. Cai, Y. Zhou, J. Jiang and B. Han, *Angew. Chem. Int. Ed.*, 2023, **62**, e202305355.

23 Y. Liu, L. Li, Z. Sang, H. Tan, N. Ye, C. Sun, Z. Sun, M. Luo and S. Guo, *Nat. Synth.*, 2024, **3**, 134-141.

24 H. Yan, Y. Peng, Y. Huang, M. Shen, X. Wei, W. Zou, Q. Tong, N. Zhou, J. Xu, Y. Zhang, Y. Ye and G. Ouyang, *Adv. Mater.*, 2024, **36**, 2311535.

25 J. Qiu, K. Meng, Y. Zhang, B. Cheng, J. Zhang, L. Wang and J. Yu, *Adv. Mater.*, 2024, **36**, 2400288.

26 J. Chang, Q. Li, J. Shi, M. Zhang, L. Zhang, S. Li, Y. Chen, S. Li and Y. Lan, *Angew. Chem. Int. Ed.*, 2023, **135**, e202218868.

27 Y. Chen, R. Liu, Y. Guo, G. Wu, T. C. Sum, S. Yang and D. Jiang, *Nat. Synth.*, 2024, **3**, 998-1010.

28 L. Zhang, C. Wang, Q. Jiang, P. Lyu and Y. Xu, *J. Am. Chem. Soc.*, 2024, **146**, 29943-29954.

29 C. Feng, J. Luo, C. Chen, S. Zuo, Y. Ren, Z. Wu, M. Hu, S. Ould-Chikh, J. Ruiz-Martínez, Y. Han, and H. Zhang, *Energy Environ. Sci.*, 2024, **17**, 1520-1530.

30 X. Zhang, H. Su, P. Cui, Y. Cao, Z. Teng, Q. Zhang, Y. Wang, Y. Feng, R. Feng, J. Hou, X. Zhou, P. Ma, H. Hu, K. Wang, C. Wang, L. Gan, Y. Zhao, Q. Liu, T. Zhang and K. Zheng, *Nat. Commun.*, 2023, 14, 7115.

31 X. Chi, Z. Zhang, M. Li, Y. Jiao, X. Li, F. Meng, B. Xue, D. Wu and F. Zhang, *Angew. Chem. Int. Ed.*, 2025, **137**, e202418895.

32 H. Peng, H. Yang, J. Han, X. Liu, D. Su, T. Yang, S. Liu, C. Pao, Z. Hu, Q. Zhang, Y. Xu, H. Geng and X. Huang, *J. Am. Chem. Soc.*, 2023, **145**, 27757-27766.

33 H. He, Z. Wang, J. Zhang, S. Mamatkulov, O. Ruzimuradov, K. Dai, J. Low and Y. Li, *Energy Environ. Sci.*, 2025, **18**, 6191-6201.

34 Y. Deng, W. Liu, R. Xu, R. Gao, N. Huang, Y. Zheng, Y. Huang, H. Li, X. Kong and L. Ye, *Angew. Chem. Int. Ed.*, 2024, **63**, e202319216.

35 P. Das, G. Chakraborty, J. Roeser, S. Vogl, J. Rabeah and A. Thomas, *J. Am. Chem. Soc.*, 2023, **145**, 2975-2984.

36 H. Xu, Y. Wang, Y. Xu, Q. Wang, M. Zhuang, Q. Liao and K. Xi, *Angew. Chem. Int. Ed.*, 2024, **136**, e202408802.

37 P. Liu, T. Liang, Y. Li, Z. Zhang, Z. Li, J. Bian and L. Jing, *Nat. Commun.*, 2024, **15**, 9224.

38 C. Bai, L. Liu, J. Chen, F. Chen, Z. Zhang, Y. Sun, X. Chen, Q. Yang and H. Yu, *Nat. Commun.*, 2024, **15**, 4718.

39 X. Zhang, D. Gao, B. Zhu, B. Cheng, J. Yu and H. Yu, *Nat. Commun.*, 2024, **15**, 3212.

40 L. Cao, C. Wang, H. Wang, X. Xu, X. Tao, H. Tan and G. Zhu, *Angew. Chem. Int. Ed.*, 2024, **136**, e202402095.

41 Y. Tang, X. Luo, R. Xia, J. Luo, S. Peng, Z. Liu, Q. Gao, M. Xie, R. Wei, G. Ning and D. Li, *Angew. Chem. Int. Ed.*, 2024, **63**, e202408186.

42 J. Wang, K. Song, T. Luan, K. Cheng, Q. Wang, Y. Wang, W. Yu, P. Li and Y. Zhao, *Nat. Commun.*, 2024, **15**, 1267.

43 C. Cheng, J. Yu, D. Xu, L. Wang, G. Liang, L. Zhang and M. Jaroniec, *Nat. Commun.*, 2024, **15**, 1313.

44 P. Das, J. Roeser and A. Thomas, *Angew. Chem. Int. Ed.*, 2023, **135**, e202304349.

45 W. Wu, Z. Li, S. Liu, D. Zhang, B. Cai, Y. Liang, M. Wu, Y. Liao and X. Zhao, *Angew. Chem. Int. Ed.*, 2024, **63**, e202404563.

46 Z. Wang, M. Li, S. Liang, Y. Kong, C. Wang, L. Li, J. Xu and Y. Yang, *J. Am. Chem. Soc.*, 2025, **147**, 13618-13628.

47 B. Feng, Y. Liu, K. Wan, S. Zu, Y. Bei, X. Zhang, M. Qiao, H. Li and B. Zong, *Angew. Chem. Int. Ed.*, 2024, **136**, e202401884.

48 K. Zhang, L. Tian, J. Yang, F. Wu, L. Wang, H. Tang and Z. Liu, *Angew. Chem. Int. Ed.*, 2023, **63**, e202317816.

49 L. Fang, H. Xu, S. Qiu, T. Ye, T. Wang, J. Shang, C. Gu, S. Kitagawa and L. Li, *Angew. Chem. Int. Ed.*, 2025, **64**, e202423220.

50 T. Yang, Y. Jin, Y. Wang, A. Kong, Y. Chen, Y. Zou, C. Liu, G. Wei and C. Yu, *Adv. Funct. Mater.*, 2023, **33**, 2300714.

51 Y. Hou, P. Zhou, F. Liu, Y. Lu, H. Tan, Z. Li, M. Tong and J. Ni, *Angew. Chem. Int. Ed.*, 2024, **136**, e202318562.